frontiers | Frontiers in Earth Science

TYPE Original Research
PUBLISHED 26 March 2025
DOI 10.3389/feart.2025.1516970

OPEN ACCESS

EDITED BY
Weichao Yan,
Ocean University of China, China

REVIEWED BY
Qibin Lin,
University of South China, China
Gang Cheng,
North China Institute of Science and Technology, China

*CORRESPONDENCE
Wulin Lei,
xakjdxwl@163.com

RECEIVED 25 October 2024
ACCEPTED 20 February 2025
PUBLISHED 26 March 2025

CITATION
Lei W, Chai J, Zheng C, Zhao J, Wang S, Liu G, Zhang J and Yang R (2025) Research on the spatiotemporal evolution of deformation and unloading mechanical effects in underlying coal and rock during upper protective layer mining.
Front. Earth Sci. 13:1516970.
doi: 10.3389/feart.2025.1516970

Research on the spatiotemporal evolution of deformation and unloading mechanical effects in underlying coal and rock during upper protective layer mining

Wulin Lei[1]*, Jing Chai[2], Chao Zheng[1], Jian Zhao[1], Siyang Wang[1], Guixian Liu[3], Jufeng Zhang[1] and Rili Yang[1]

[1]School of New Energy, Longdong University, Qingyang, Gansu, China, [2]College of Energy Engineering, Xi'an University of Science and Technology, Xi'an, China, [3]School of Literature and History, Longdong University, Qingyang, Gansu, China

The spatiotemporal rule of pressure release in rock–coal strata within the mining zone serves as the theoretical basis for the prevention and control of dynamic disasters during the mining of the stress-concentration stratum. Taking the mining of the upper protective layer of the Hulusu coal mine located in Ordos City, Inner Mongolia Autonomous Region, China, as the engineering background, this study, based on the theory of elastic–plastic mechanics, investigates the pressure relief mechanics of the underlying coal and rock during the upper protective layer mining. The research is conducted across different scales through rock mechanics experiments, numerical simulations, and on-site industrial experiments. The spatiotemporal evolution of the stress and displacement fields in the underlying coal and rock strata during the upper protective layer mining was simulated and analyzed using the 3-Dimensional Distinct Element Code. Brillouin optical time-domain analysis distributed fiber-optic sensing technology was used to monitor the deformation and unloading dynamic process of different rock–coal strata under the mining floor in real-time. The results indicate that the stress changes in the underlying rock–coal strata during the mining of the upper stress-concentration stratum can be divided into four phases, namely, *in situ* stress, stress concentration, stress release, and stress restoration. Due to the uneven distribution of the waste rock collapse in the mined-out area, stress is alternately distributed in the unloading stable zone, unloading recovery zone, and boosting zone. The mining-induced stress distribution curve in the protected coal seam changes from a U-shape to a W-shape and then to a "WWW"-shape. The stress-relieving effect of upper stress-concentration stratum mining is significant, but the stress-relieving parameters vary depending on time and spatial factors. The research results have important theoretical and practical significance for guiding the layout and key parameter design of stress-concentration stratum mining.

KEYWORDS

upper stress-concentration stratum, stress-relieving effect, rock mechanics tests, numerical simulation, field monitoring

1 Introduction

With the shallow coal resources being depleted, deep coal development has become the norm (Li et al., 2020; Kang et al., 2023; Zhu et al., 2021). However, deep coal resources are affected by high *in situ* stress, which leads to frequent mine dynamic disasters. Thus, the complex stratum environment becomes difficult to predict and control, posing challenges to the safety of working in many mines (Yu et al., 2018; Xu L. et al., 2019; Xie et al., 2019). Mining stress-concentration strata is one of the most economically effective measures for preventing and controlling mining-induced dynamic disasters in many coal seams. It has a wide range of applications in several mines across China (Lei et al., 2024; Liu et al., 2022; Liu et al., 2023). The mining of stress-concentration strata can change the stress distribution within the rock–coal structure, release the elastic energy from strata extrusion, and damage the wall rock structure, effectively preventing and controlling the intensity of dynamic disasters at the source (Shen et al., 2017; Xiao et al., 2019; Li et al., 2021).

In recent years, the frequent occurrence of rockburst disasters in mines has attracted widespread attention from scholars both at home and abroad. Yuan et al. (2024) introduced cloud model theory for the prediction of rockburst intensity levels and ultimately established a comprehensive evaluation model for rockburst intensity based on the BO-XGBoost cloud model. Wang et al. (2024) proposed a backpropagation neural network (BPNN) prediction model based on surface subsidence data to address the frequent occurrence of high-energy microseismic events in coal mines, providing a basis for safe and effective prediction of coal mine disasters. Lv et al. (2024) proposed a new prevention and control method based on hydraulic fracturing and conducted a sensitivity analysis on key parameters such as geostress, roof solidity coefficient, flow increment, and borehole spacing to evaluate their impact on the hydraulic fracturing effect. Yang (2024) successfully used random forest and Mann–Kendall trend testing methods to identify and predict precursor characteristic signals of coal mine rockburst. Mu et al. (2024) used FLAC3D's dynamic module to simulate and analyze the effects of propagation distance, overburden structure in multi-seam mining, and interlayer plastic zones on vibration wave attenuation. Sitao et al. (2021) analyzed the stress changes and energy release laws of the working face advancement and fault zone, revealing the rockburst mechanism under the coupling effect of square and regional structural stresses in the working face. Stress-concentration stratum mining technology was first applied to coal or gas outburst control in France, Germany, Poland, and other countries in 1930 (Cundall PA, 1976; Banerjee, 1987; Blair and Cook, 1998), and it was not until 1980 that it was gradually adopted for controlling the intensity of dynamic disasters such as rockburst (Lan et al., 2016; Jiang and Zhao, 2015). Most scholars believe that the mechanism of stress-concentration stratum mining for controlling dynamic disasters is closely related to factors such as rock–coal structure, rock–coal strata migration, stress distribution in the mining zone, and spatiotemporal effects (Cao et al., 2018; Xuanhong et al., 2024). Li et al. (1997) analyzed the anti-erosion effect and protection parameters of stress-concentration stratum mining in the Huafeng coal mine. Guan et al. (2002) studied the displacement, stress, and other changes in the rock–coal mass during the mining of steeply inclined stress-concentration coal stratum, as well as the extent of the protection range. Zhu et al. (2003) studied the dynamic process and stress-relief range of the development of fracture zones while mining the steeply inclined stress-concentration stratum in the Datai well. Tu et al. (2007) studied the stress distribution characteristics and pressure relief range of the protected layer during long-distance underground mining. Shen et al. (2011) analyzed the feature of stress transfer from lower stress-concentration stratum mining to the deep coal body. Sun et al. (2013) studied the stress variation trait of the rock body on the mining floor using the stress–strain test method. Xiong et al. (2014) divided the protected layer into five zones along the strike direction, namely, compression zone, depressurization expansion zone, depressurization expansion stable zone, depressurization expansion zone, and compression zone. Pang et al. (2016) numerically simulated and studied the elastic zone, velocity, stress, and plastic zone under the influence of the dynamic load disturbance stress of the same strength when the upper protection layer was not mined and after mining. Zhang et al. (2017) researched the development of cracks, stress state, expansion deformation, and changes in permeability characteristics in the protected coal seam. Jiang et al. (2019) proposed stress criteria for impact and large deformation boundaries under different widths of local stress-concentration strata. Tian et al. (2014), Li et al. (2012), Guan et al. (2008), and Gong et al. (2005) studied the dynamic change feature of stress in the rock–coal strata of the bottom plate during the mining process of the stress-concentration stratum through physical simulation experiments and obtained a W-shaped curve characteristic of stress distribution in the protected coal seam along the strike direction under the influence of mining. Xu G. et al. (2019), Chen et al. (2013), and Dai et al. (2013) used numerical simulation software to construct a large three-dimensional ore body. Their findings indicate that the vertical stress in the middle of the mined-out area is superimposed in multiple V-shapes, while the horizontal stress is superimposed in multiple A-shapes. Yuan et al. (2019) used multiple regression analysis to study the protective effect of stress-concentration stratum mining at different interlayer intervals. Fang et al. (2020) researched the stress-relieving range of stress-concentration stratum mining under different dip angles using similarity simulation research methods. Lin et al. (2021) studied that the failure mechanism of the sample is mainly caused by crack propagation in the low-strength layer. Shi et al. (2022) analyzed the relationship between mining height and the stress-relieving effect of the protected coal seam. Chen et al. (2024) researched the impact of long-distance mining of residual coal pillars in the stress-concentration stratum on the recovery of the protected coal seam. Liu et al. (2023) utilized numerical simulation methods to study the stress distribution and evolution rule of wall rock after the mining of upper and lower stress-concentration strata. For a long time, research on stress-concentration stratum mining has mainly focused on the qualitative analysis of coal seam stress relief, gas extraction, and stress changes in the protected coal seam, without considering the dynamic relationship between mining-induced stress in time and space and rarely involving quantitative research on pressure relief parameters.

Therefore, with the Hulusu mine as the research background, by combining 3DEC simulation with BOTDA monitoring, the advantages of both can be fully utilized to achieve complementarity between numerical simulation and real-time monitoring. 3DEC

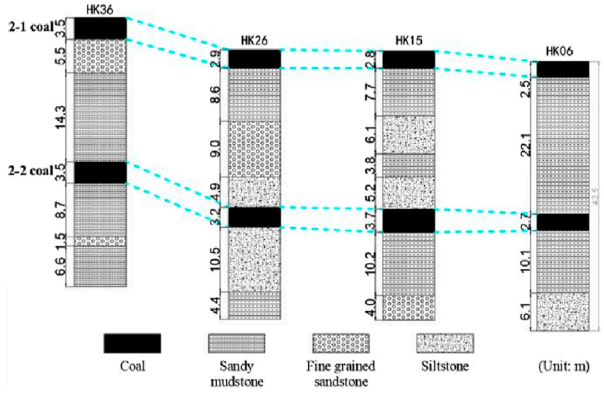

FIGURE 1
Schematic diagram of changes in the distribution of roof and floor rock properties of coal seams 2-2 and 2-1.

simulation can provide theoretical predictions of coal rock deformation and stress distribution, while BOTDA monitoring can verify these predictions and provide real-time deformation data. This combination can significantly improve the accuracy and reliability of coal and rock deformation monitoring, providing a more accurate scientific basis for engineering practice. The spatiotemporal evolution feature of the stress zone and displacement field of the underlying rock–coal strata during upper stress-concentration stratum mining is studied. On this basis, the spatiotemporal relationship of the stress-relieving effect of the protected coal seam is explored. Parameters such as pressure relief angle, depth, and range are obtained. The research results contribute to a systematical understanding the influence of coal seam occurrence conditions on the protective effect of protective layer mining, providing a theoretical and scientific basis and technical guidance for the scientific and reasonable development layout design of close-range coal seam groups in rockburst-induced mines. It is of great significance for improving the safety of protective layer mining design and refining the theory of protective layer mining, and preventing and controlling rockburst disasters in the Hulusu mine and surrounding areas.

2 Overview of mines

The Hulusu coal mine in Inner Mongolia is selected as the experimental mine. The 2-1 coal seam and 2-2 coal seam in this mine have a strong impact tendency, with average thicknesses of 2.5 m and 3.9 m, respectively, average burial depths of approximately 639 m and 658 m, respectively, and an average inclination angle of 2°. The interlayer lithology of the two layers of coal is mainly composed of sandy mudstone, fine-grained sandstone, and siltstone, all of which have a weak impact tendency, with a spacing range of 19.19 m–23.73 m, as shown in Figure 1. The upper 2-1 coal seam was mined first, followed by the lower 2-2 coal seam. Therefore, mining the 2-1 coal seam would release some concentrated stress above the 2-2 coal seam, allowing us to define the 2-1 coal seam as the stress-concentration stratum for the 2-2 coal seam.

The experimental work zone mainly mines the 2-1 coal seam, with a strike length of 3,015 m, a dip length of 320 m, and a mining height of 3.9 m. The work zone advances eight times a day, with each cut of 0.8 m and a daily pushing progress of 6.4 m. The monthly effective working days are 27.5 days, and the monthly pushing progress is 190.3 m. The service life is 17.4 months. The mining method is the longwall backward mining method. In addition, the entire collapse method is used to treat the roof of the mined-out area.

3 Rock–coal stratum physical and mechanical parameter testing

The coal samples used in the test were taken from the heading face of the 2-2 coal seam in the Hulusu coal mine, with a buried depth of approximately 660 m and a coal seam thickness of approximately 3.86 m. The collected coal samples were sealed with plastic film and plastic foam to prevent the coal and rock from breaking during transportation. The coal sample is black in color, with brownish-black stripes, stepped fractures, and layered structures. The macroscopic coal rock composition is mainly composed of bright coal, followed by dark coal and visible filamentous coal. The organic microscopic components of coal samples are mainly composed of inertinite and vitrinite, with a small amount of shell.

According to the "method for determining the physical and mechanical properties of coal and rock," the test specimens are processed into standard cylindrical specimens with a diameter of 50 mm and a height of 100 mm after drilling, sawing, and grinding processes. The test piece must ensure that both ends are parallel, smooth, and free of significant scratches. The parallelism of the two end faces should be less than 0.02 mm, the flatness should be less than 0.5 mm, and the diameter deviation should be less than 0.02 mm. The processing accuracy of the test piece must meet the requirements of the national standard for rock mechanics testing. The apparent density of rock–coal mass was measured using electronic tray scales, Vernier calipers, and other equipment, with the average value obtained from multiple measurements. A microcomputer-controlled electronic universal testing machine was used to determine mechanical parameters such as rock and coal strength, friction angle, cohesion, and Poisson's ratio. The parameters are shown in Table 1.

4 Model establishment and excavation

The numerical simulation software 3DEC is a three-dimensional discrete element method program that can simulate the discontinuous discrete characteristics of surrounding rocks in goaf areas. It can realistically achieve failure phenomena such as mutual shear and displacement or detachment of overlying rocks in goaf areas, making the collapse of gangue in goaf areas cause discontinuous deformation of the underlying coal rock mass under stress, and can more realistically simulate the stress recovery process of the underlying coal rock mass in goaf areas. However, 3DEC needs to simplify the complex coal rock geological structure into a collection of blocks and assume the interaction relationships

10.3389/feart.2025.1516970

TABLE 1 Physical and mechanical parameters of rock and coal.

Category	Bulk density /kg·m^{-3}	Unidirectional compressive strength/MPa	Unidirectional tensile strength/MPa	Elastic modulus /GPa	Poisson's ratio	Adhesive strength /MPa	Internal friction angle/°
2–1 coal roof	2,386	33.73	4.24	9.81	0.18	5.5	38
2-1 coal	1,260	12.97	1.22	2.29	0.29	2.3	40
2-1 coal floor	2,501	38.31	6.15	15.05	0.24	10.9	25
2–2 coal roof	2,297	15.87	2.42	7.91	0.25	3.0	40
2-2 coal	1,269	14.67	1.21	2.63	0.259	3.1	38
2-2 coal floor	2,500	28.42	7.43	24.3	0.26	7.2	36

between blocks during numerical simulation calculations. The dynamic transmission mode of stress between the collapsed gangue and the top and bottom shale layers in the goaf is also different from that in the field, which will have a certain impact on the research results. Therefore, by taking measures such as optimizing model construction, setting reasonable physical and mechanical parameters of coal and rock masses, and optimizing calculation settings, the accuracy and reliability of 3DEC simulation can be significantly improved.

Therefore, this article adopts 3DEC simulation to simulate the full cycle process of pressure relief of the protected 2-2 coal seam under the influence of upper stress-concentration stratum (2-1 coal seam) mining. The two coal mining faces of 2-1 seam are named 1# and 2#, respectively. Based on the boundary effect of the model and a reasonable calculation time, the model dimensions are 1,200 m long, 600 m wide, and 325 m high. A coal pillar of 100 m is left at each boundary, with an excavation length of 10,000 m. A total of 30 layers of rock are formed, with a cumulative thickness of 325 m, as shown in Figure 2. Model displacement boundary conditions: displacement boundaries are used in the x-direction of the model to restrict displacement in the x-direction. Displacement boundaries are used in the y-direction to limit the displacement in the y-direction. Displacement boundaries at the bottom boundary of the model are used to limit the displacement in the z-direction. The upper boundary of the model adopts a free boundary, first simulating some overlying rock layers and then simplifying the overlying rock mass of the mined coal seam into a uniformly distributed load applied to the upper boundary instead of the gravity of the overlying rock, resulting in vertical stress. A certain gradient of horizontal stress on both sides of the model is applied, and fixed boundaries are used. The maximum initial vertical principal stress is 17.58 Mpa in the model, and the maximum initial horizontal principal stress is 21.09 Mpa. In addition, the stress coefficient is 1.1–1.3. Before excavating the model, all node displacements were reset to 0. The work zone is 320 m long, with a mining height of 7.5 m. Each excavation is 5 m, with a total of 200 excavations and a total advance length of 1,000 m.

5 Analysis of the deformation rule of rock–coal strata in the mining zone

5.1 Stress variation rule

According to the simulation results, a profile was taken along the strike direction of advancement in the middle of the 1# coal mining face of the upper stress-concentration stratum (2-1 coal seam). In addition, the stress distribution rule of the wall rock in the mining zone was obtained, as shown in Figure 3. When the moving forward distance of the work zone is between 30 m and 90 m, stress-concentration occurs in the rock–coal strata before and after the mining zone, and the distribution position is relatively fixed. There is a phenomenon of stress reduction in the mined-out area, and as the work zone advances, the range of stress reduction continues to expand and gradually decreases toward the middle of the mined-out area. When the moving forward distance of the work zone is 120 m, stress recovery occurs in the unloading zone. As the degree and range of stress recovery continue to increase, some

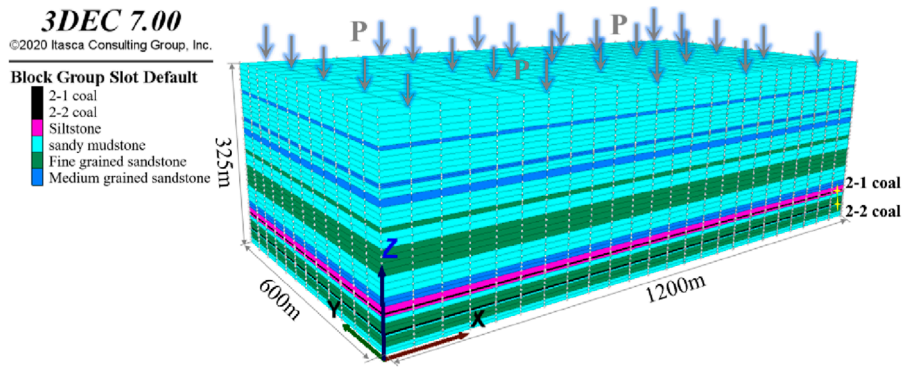

FIGURE 2
Schematic diagram of the numerical model of three-dimensional geological structure of a mine.

zones begin to change from the unloading zone to the boosting zone. When the moving forward distance of the work zone is 200 m, the stress-relieving zone is completely separated, transforming from one pressure relief zone to two pressure relief zones and one pressure relief zone. This is due to the uneven collapse of the mined-out area, which results in the formation of compacted and non-compacted waste rock zones, indicating that the stress relief effect of mining the stress-concentration stratum (2-1 coal seam) mining is time-dependent. When the moving forward distance of the work zone is 240 m, the mining reaches a fully mined state. In addition, the vertical influence range of the stress-relieving zone reaches its maximum value. At this time, the maximum depth of pressure relief reaches 32.8 m, and the distance between the maximum depth of the stress-relief zone and the work zone is 35.5 m. When the moving forward distance of the work zone is 280 m, a total of four pressure relief zones and three pressure-boosting zones are formed in the mined-out area, and they are alternately distributed.

Along the variation of the strike, after the mining of the work zone is completed, a total of 16 pressure relief zones and 17 pressure-boosting zones are formed in the mining zone. The maximum range and degree of pressure relief are located on both sides of the mined-out area, with the lowest degree of pressure relief in the middle of the mined-out area. The range and degree of pressure relief of the roof strata are larger than those of the floor strata. In addition, the stress-relieving effect gradually weakens from the mined-out area in both upward and downward directions, as shown in Figure 4A. In the dip direction, there are a total of five unloading zones and six boosting zones formed in the 1# coal mining face and four unloading zones and five boosting zones formed in the 2# coal mining face. This is because the stress-relieving zone on the coal pillar side of the 1# coal mining face is affected by the mining of the 2# coal mining face. In addition, the stress in the stress-relieving zone is restored, transforming from one pressure relief zone to two pressure relief zones and one pressure-boosting zone. The 30-m width of the coal pillar between the two working faces causes the maximum compressive stress peak to appear at the position of the coal pillar. In addition, the stress is significantly concentrated. The compressive stress is transmitted to the lower part of the bottom plate, causing the 2-2 protected coal seam below the coal pillar to become a pressurized zone. The risk of dynamic disasters in this zone is relatively high, as shown in Figure 4B.

5.2 Displacement variation rule

The displacement variation rule of the rock–coal strata in the mining zone along the strike direction is shown in Figure 5A. The roof collapse of the mined-out area is uneven, with the alternating distribution of fully collapsed and compacted zones and non-fully collapsed zones, resulting in different compression deformation effects of collapsed waste rock on the bottom plate, which leads to inconsistent recovery of bottom plate deformation within the mined-out area range. The maximum sinking amount of the mined-out area roof is 2.51 m. In addition, the maximum floor heave is 0.258 m. The bottom plate in the fully collapsed zone is subjected to significant compression deformation. The deformation of the floor bulge in the intermediate position of the mined-out area is significantly restored. The bottom plate in the zone with insufficient collapse is less affected by compression deformation, and the deformation recovery of the bottom bulge on both sides of the mined-out area is weaker. The displacement variation rule of rock–coal strata in the dip direction mining zone is shown in Figure 5B. The displacement changes in the mined-out area are symmetrically distributed, with a small sinking amount of displacement of the roof on both sides and a large sinking amount of the middle roof. The displacement characteristics of the roof and floor of the two working faces are basically the same, but the displacement of the roof and floor of the 2# coal mining face is significantly larger than that of the 1# coal mining face after mining. In addition, the 30-m-wide coal pillar undergoes compression and deformation, causing regional stress concentration and the propagation of compressive stress to the bottom plate. This, in turn, results in stress concentration in the protected coal seam directly beneath the coal pillar.

6 Mechanical analysis of the rule of pressure relief under protection

To quantitatively analyze the stress variation rule of the 2-2 protected coal seam after stress-concentration stratum mining (2-1 coal seam), 241 measuring points were set up along the strike direction of the protected coal seam to quantitatively analyze the

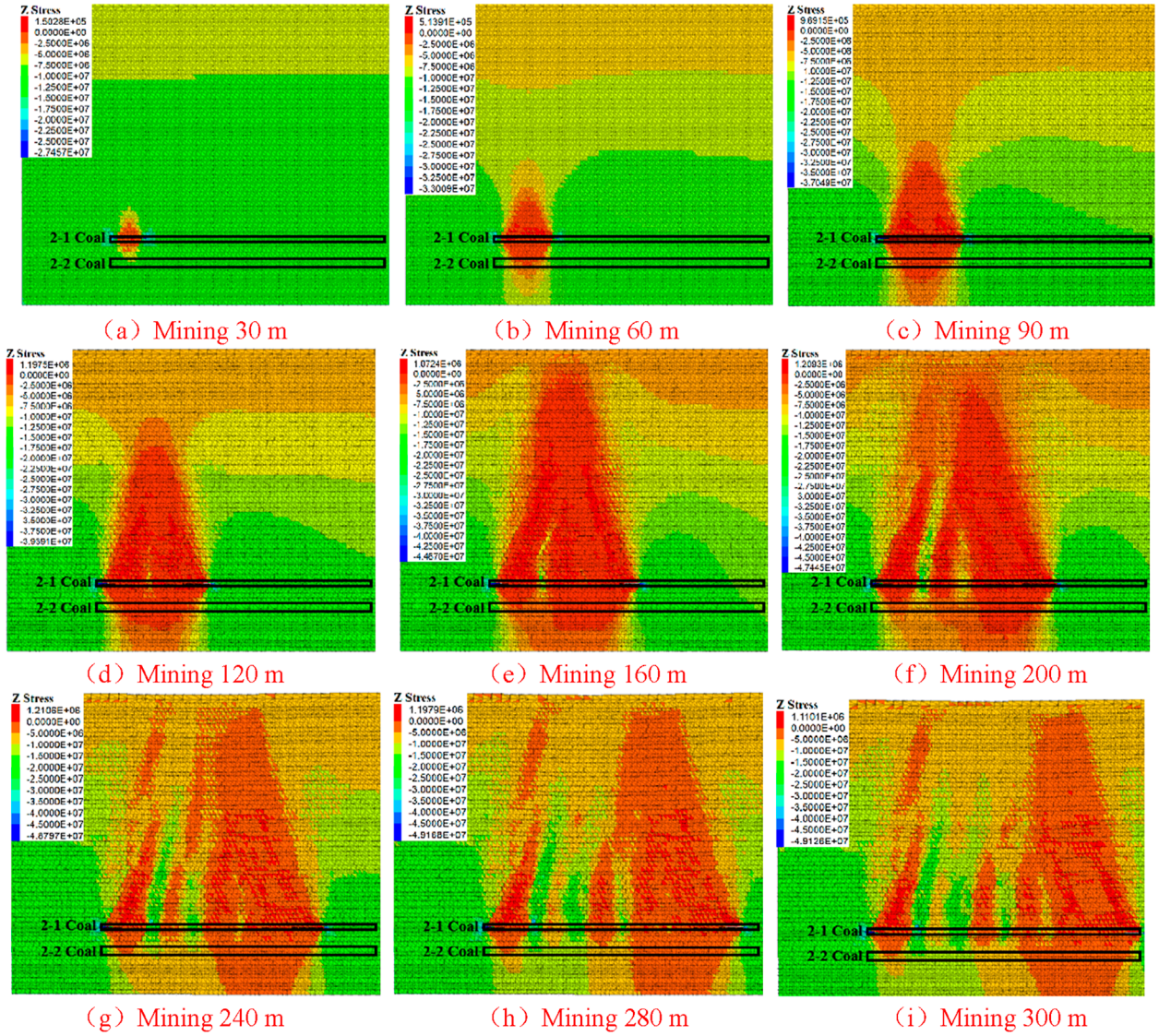

FIGURE 3
Stress distribution in the mining area during the mining process of the upper protective layer 2-1 coal and stress variation cloud map of the protected 2-2 coal: **(A)** mining 30 m, **(B)** mining 60 m **(C)** mining 90 m, **(D)** mining 120 m, **(E)** mining 160 m, **(F)** mining 200 m, **(G)** mining 240 m, **(H)** mining 280 m, and **(I)** mining 300 m.

stress variation rule of the 2-2 coal seam during the 2-1 coal seam mining process. The vertical compressive stress is positive, while the tensile stress is negative. The compression deformation of vertical displacement is negative, while the expansion deformation is positive.

6.1 Distribution rule of induced stress

With the mining of the upper stress-concentration stratum (2-1 coal seam), the strain change curve of the protected coal seam (2-2 coal seam) can be divided into three parts, namely, the stress increase zone, the stress decrease zone, and the *in situ* stress zone. When the moving forward distance of the work zone is 10 m, the stress-relieving effect of the protected coal seam begins to emerge, and as the work zone advances, the stress-relieving effect becomes more and more significant. When the moving forward distance of the work zone is 80 m, the first minimum stress peak of the protected coal seam is 1.29 MPa, and the step distance of the first unloading peak is 80 m. As the work zone continues to advance, the peak value of the minimum stress moves forward along the strike direction and begins to increase. This is because the stress in the unloading zone gradually recovers due to the stress disturbance of the collapse of the overburden in the mined-out area, indicating that the unloading of the stress-concentration stratum is time-dependent. When the moving forward distance of the work zone is 140 m, some stress in the unloading zone has been restored to the *in situ* stress or high-stress state, and the unloading zone has transformed into a stable or pressurized unloading zone. The initial unloading recovery step distance is 140 m. When the moving

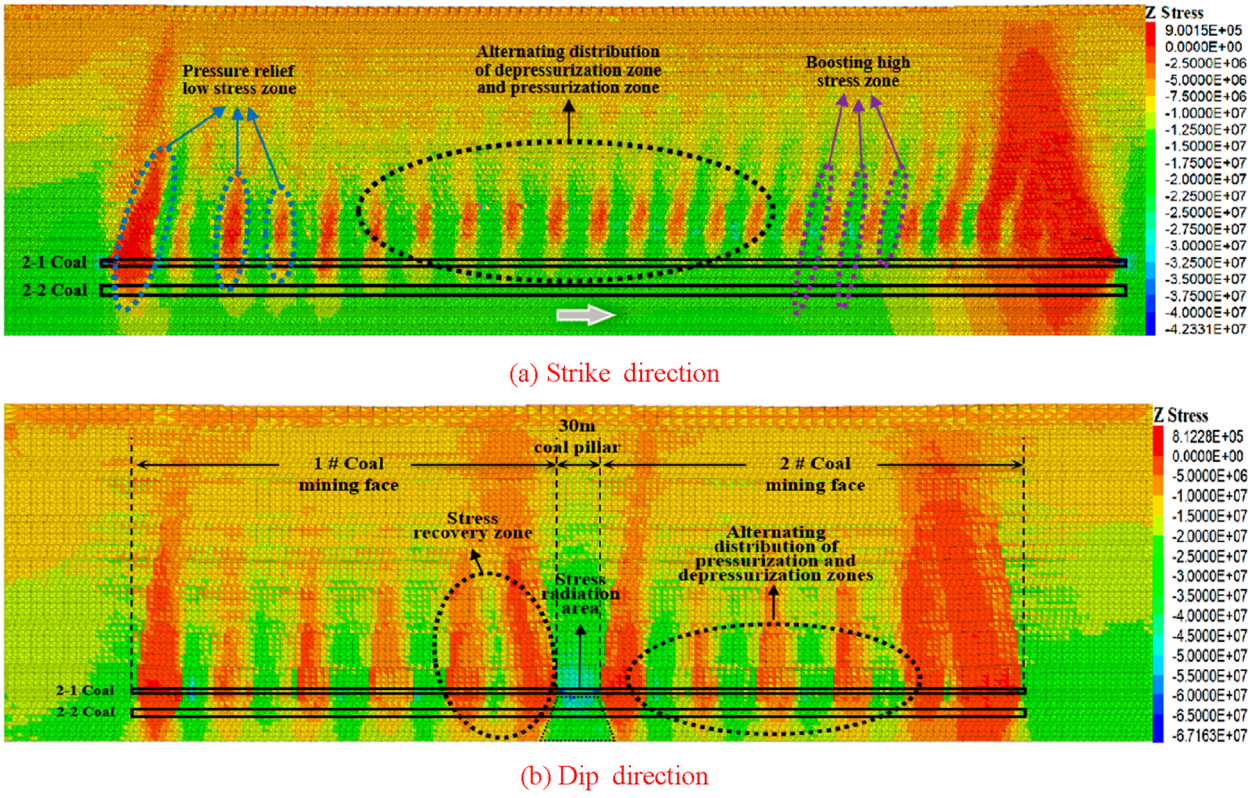

FIGURE 4
Visualization cloud diagram of stress distribution in the mining area after the completion of the mining of the 1 # and 2 # working faces of the upper protective layer 2-1 coal: **(A)** strike direction and **(B)** dip direction.

forward distance of the work zone is 200 m, the third minimum stress peak appears in the protected coal seam, and the step distance of the unloading peak is 60 m. When the moving forward distance of the work zone is 210 m, the distance from the unloading zone to the boosting zone for the second time is 70 m, and the recovery distances for the two unloading zones are 140 m and 70 m, respectively. Therefore, the reasonable unloading distance should be less than 70 m, and the unloading protection effect is most significant. As the work zone moves forward, the stress-relieving zone continuously moves forward along the strike direction of advancement, and the stress in the protected coal seam undergoes dynamic processes of initial increasing, gradually decreasing, then increasing, and recovering. When the mining range of the stress-concentration stratum is small, the vertical stress distribution curve of the protected coal seam takes on a U-shape. As the mining range of the stress-concentration stratum gradually increases, the vertical stress distribution curve gradually changes from a U-shape to a W-shape. As the mining space further increases, the vertical stress distribution curve changes from a W-shape to a "WWW"-shape, as shown in Figure 6.

According to the stress variation rule of coal in the 2-2 protected coal seam, parameters such as the initial unloading peak step distance, periodic unloading peak step distance, and unloading recovery step distance can be obtained when the protection layer mining reaches the maximum unloading effect. For details, please refer to Table 2.

The quantitative analysis of the stress changes of the protected coal seam (2-2 coal seam) is shown in Figure 7. The red zone in the figure represents the pressurization zone, the green zone represents the depressurization zone, and the blue zone represents the fully depressurized zone. If the stress release rate exceeds 10%, serving as the unloading index, the unloading angles of the protected coal seam along the direction of the strike are 79.1° and 80.2°, and the cumulative range of the unloading zone of the protected coal seam is 555 m, accounting for 55.4% of the mined-out area range. The unloading angles of the protected coal seam in the dip-inclined direction after mining at the 1# coal mining face are 59.5° and 70.3°, and the cumulative range of the unloading zone is 112.8 m, accounting for 35.2% of the mined-out area range. The stress-relieving angles of the protected coal seam in the dip direction after mining at the 2# coal mining face are 73.6° and 69.7°, and the cumulative pressure relief range in the mined-out area is 147.9 m, accounting for 46.1% of the mined-out area range.

6.2 Mining-induced stress path effect

Through an in-depth analysis of the mining stress rule of the protected coal seam, the mining stress can be divided into two categories. The first category is any point on the boundary of the mined-out area, and the entire process of stress change at that point can be divided into four phases, as shown in Figure 8A. The

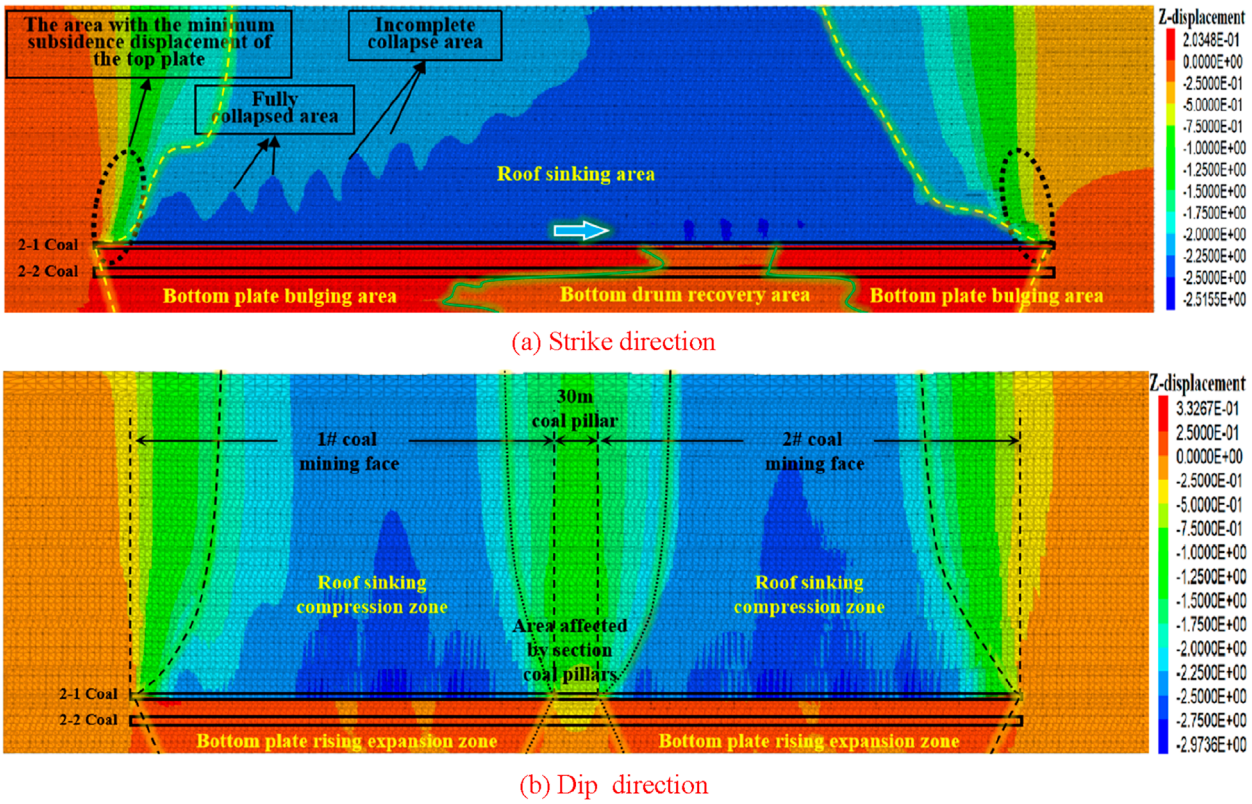

FIGURE 5
Visualization cloud diagram of displacement distribution in the mining area after the completion of the mining of the 1 # and 2 # working faces of the upper protective layer 2-1 coal: **(A)** strike direction and **(B)** dip direction.

OB area is a low-stress phase, located below the coal wall of the work zone in the early phase of mining. Due to the short mining distance, the stress concentration in the mining zone is low, and the stress transmitted to the 2-2 coal seam (the protected coal seam) is also low. Point A is the maximum stress peak. The BC area is in the phase of stress relief development. After the work zone passes through this point, it is located below the mined-out area. As the work zone moves forward, the stress continuously decreases. Point C is the minimum stress peak, indicating the most optimal time and space state for stress relief. Due to its location at the boundary of the mined-out area, the roof collapse of the mined-out area is insufficient, and the degree of stress relief recovery is relatively low. The DE area is the phase of stress relief and stability. Due to the stable deformation of the wall rock in the mined-out area, the stress at this point remains basically stable as the work zone advances. As shown in Figure 8B, the second type is any point in the middle of the mined-out area, and the entire process of stress change at that point can also be divided into four phases. Stage OB is the phase of high stress, and mining is more thorough due to the distance from the cutting eye. Therefore, the changing process of stress can be divided into three parts, namely, unaffected in the initial phase, slow growth in the middle phase, and rapid decline in the later phase. The BC area is in the phase of stress relief development, so the stress in the mining zone transfers to both sides of the mined-out area, resulting in a continuous decrease. The CD area is in the phase of full stress recovery, characterized by a large mining space and significant collapse of the overlying strata. The mined-out area is gradually filled and compacted by waste rock, so the basic top rotation deformation contacts the waste rock. The geostatic stress of the overburden is applied to the bottom rock stratum, and the stress of the protected coal seam is fully restored. At point D, the vertical stress foundation quickly recovers to the level of the *in situ* stress, or at point D1, the vertical stress exceeds the *in situ* stress. The DE phase is the stable phase of stress relief.

6.3 Evolution rule of mining-induced stress and displacement

There are some internal relationships between displacement field variation and stress field characteristics of the protected coal seam (2-2 coal seam) during the mining process of the upper stress-concentration stratum (2-1 coal seam). Along the variation of the strike, the peak position of the displacement curve can correspond to the valley position of the stress curve, and the valley position of the displacement curve can correspond to the peak position of the stress curve, indicating that the greater the displacement of the protected coal seam, the more severe its expansion deformation, so the better the stress-relieving effect. The smaller the displacement of the protected coal seam, the smoother its expansion deformation, resulting in a weaker stress-relieving effect, as shown in Figure 9A. In dip inclination, the relationship

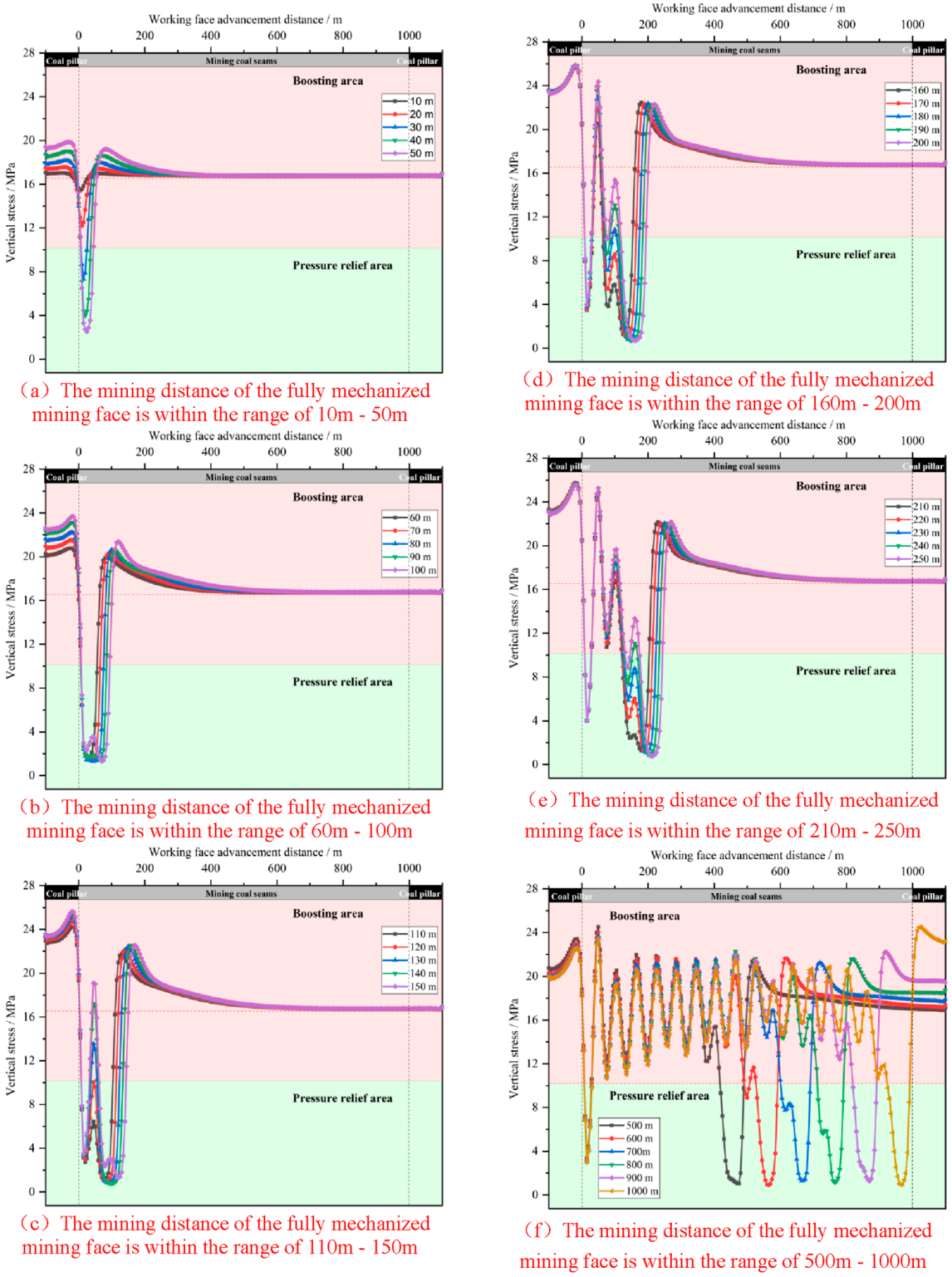

FIGURE 6
Stress variation pattern of coal in the lower protective layer 2-2 during the mining process of the upper protective layer 2-1. **(A)** The mining distance of the fully mechanized mining face is within the range of 10 m–50 m. **(B)** The mining distance of the fully mechanized mining face is within the range of 60 m–100 m. **(C)** The mining distance of the fully mechanized mining face is within the range of 110 m–150 m. **(D)** The mining distance of the fully mechanized mining face is within the range of 160 m–200 m. **(E)** The mining distance of the fully mechanized mining face is within the range of 210 m–250 m. **(F)** The mining distance of the fully mechanized mining face is within the range of 500 m–1,000 m.

TABLE 2 Parameters related to the pressure relief of stress-concentration stratum.

Classification	Parameter/m
Peak step distance for initial pressure relief	80
Peak step distance for periodic pressure relief	60~80
Recovery step distance for initial pressure relief	140
Recovery step distance for periodic pressure relief	70~80

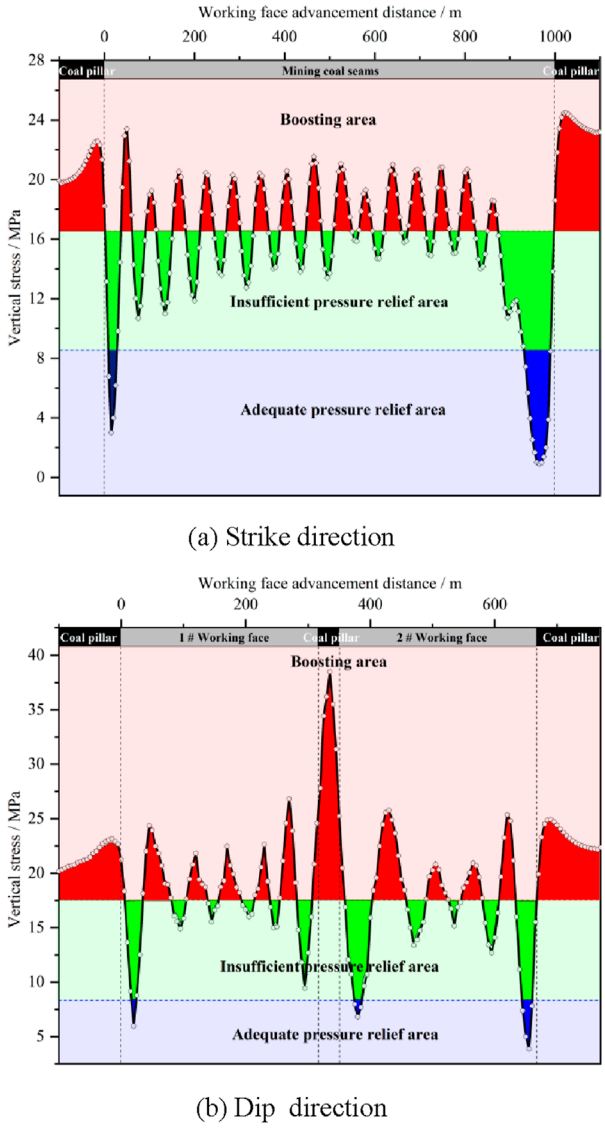

FIGURE 7
Distribution pattern of the depressurization and pressurization zones of 2-2 coal in the protected layer during the mining process of the upper protective layer: **(A)** strike direction and **(B)** dip direction.

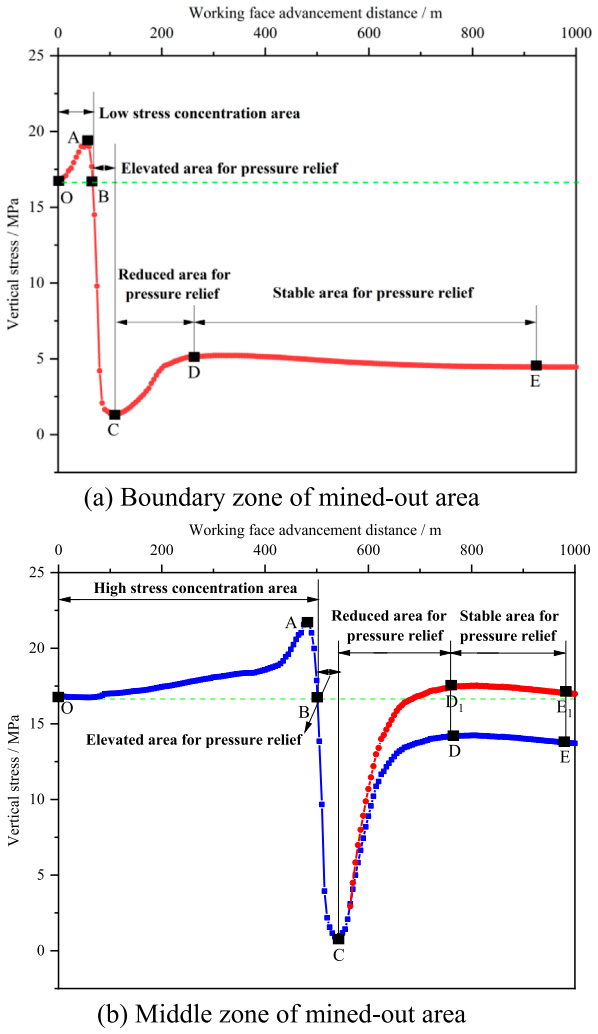

FIGURE 8
Schematic diagram of the entire process curve of mining stress for the protected layer 2-2 coal: **(A)** boundary zone of mine and **(B)** middle zone of the mined-out area.

between the displacement field and stress field changes is basically consistent with the direction of the strike. The displacement at the coal pillar reaches its minimum peak, while the stress reaches its maximum peak. The stress field and displacement field change amplitude are the largest in the zone affected by the coal pillar, as shown in Figure 9B.

7 Engineering measurement

The on-site monitoring of the mine adopts distributed fiber-optic sensing technology and Brillouin optical time-domain analysis technology based on stimulated Brillouin scattering. The spatial resolution is 5 cm, the sampling interval is 1 cm, and the testing range is 95.37 m in direction, 128.47 m in inclination, and 36.94 m in vertical direction. Three boreholes, namely, 1 #, 2 #, and 3 #, were drilled toward the bottom plate of the main transportation roadway in the 21104 working face. The azimuth angle of borehole

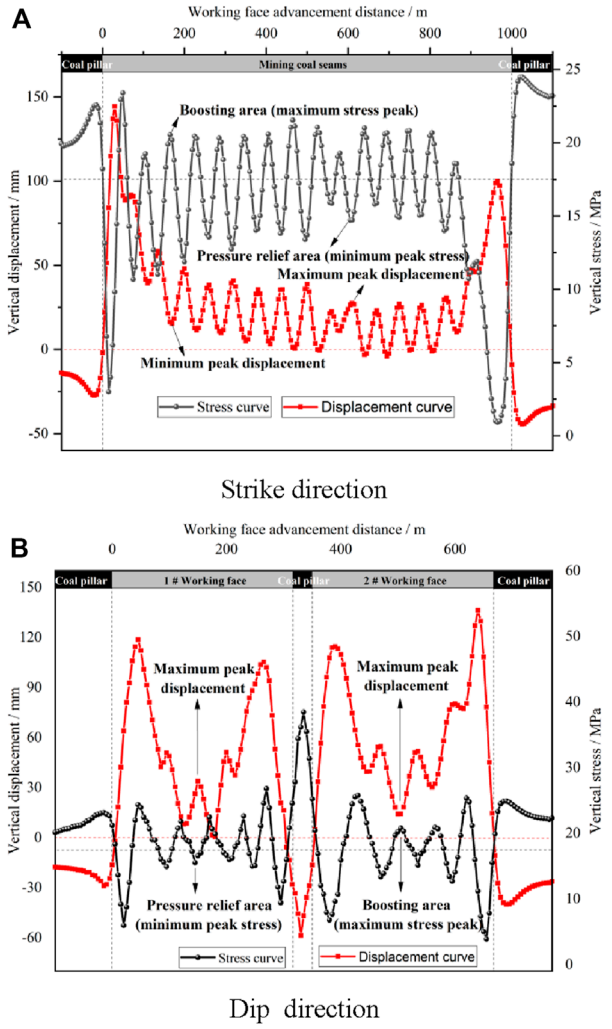

FIGURE 9
Comparison diagram of the changes in the mining stress and displacement of the protected layer 2-2 coal during the mining process of the upper protective layer. **(A)** Strike direction. **(B)** Dip direction.

1 # is 270°, the inclination angle is 15°, and the borehole length is 133.00 m. The azimuth angle of hole 2 is 270°, the inclination angle is 45°, and the hole length is 37.00 m. The azimuth angle of hole 3 is 200°, the inclination angle is 20°, and the hole length is 108.00 m. Fiber optic cables are implanted in the borehole, and metal-based cable-shaped optical cables are used as fiber optic sensors, which have superior tensile performance and good coupling with rock layers. The installation process of the fiber optic monitoring system consists of four steps, namely, fiber optic hole positioning and construction, fiber optic sensor implantation drilling, fiber optic hole grouting, and monitoring system connection. The fiber optic implantation method adopts the coupling method of drilling and grouting throughout the entire section, the spatial positioning adopts the micro-bending event method, and the data denoising processing adopts the wavelet threshold method. As the working face advances, data are continuously collected and analyzed until the mining impact range moves beyond the fiber-optic sensor or the deformation of the surrounding rock stabilizes. In other words, the fiber-optic sensor strain data remain stable and unchanged, marking the end of monitoring. (Figure 10)

Lei et al. (2022) conducted a real-time analysis on the stress data of the underlying rock–coal strata during the mining process of the upper stress-concentration stratum (2-1 coal seam) in the Hulusu mine. The results show that the maximum unloading depth along the direction of the strike is 28.4 m, and the length between the maximum unloading depth location and the horizontal distance of the work zone is approximately 38.5 m–40.5 m. The unloading lag distance of the protected coal seam is 14.3 m. The unloading angle of the protected coal seam along the direction of the strike is 63.6°, which is 58.7° in the dip direction. The unloading ratio of the protected coal seam along the direction of the strike is 63.4%–84.7%, which is 43.5%–63.4% in the dip direction. The numerical calculation and engineering measurement results of the stress-relieving parameters for the upper stress-concentration stratum mining are shown in Table 3, and the trend of parameter changes is basically consistent. However, the numerical simulation analysis shows a larger stress-relieving angle than that of engineering measurements, and the results of the stress-relieving ratio and pressure relief lag distance are smaller than those measured in engineering. This discrepancy arises because numerical simulations account for the deformation of the rock–coal strata in the mining zone more comprehensively.

8 Discussion

In order to compare and observe the stress change pattern of 2-2 coal throughout the whole mining process, 20 stress change curves were plotted at intervals of 50 m for different advance distances, with the trough representing the pressure relief area and the peak representing the pressure increase area, as shown in Figure 11. As shown in the figure, the depressurization and pressurization zones are alternately distributed in the goaf, and the depressurization zone shows an uneven distribution pattern. As the working face advances along the direction of the strike, the pressure relief zone continuously moves forward along the direction of the strike, and the pressurization zone in front of the coal wall gradually transforms into the pressure relief zone. The working face continues to advance, with a portion of the pressure relief zone transforming into a pressure-boosting zone, while the degree of pressure relief in the other portion decreases. The pressure relief range of the entire mining process continues to increase, and the maximum pressure relief zone is always located on the side of the goaf near the coal wall.

A comparative analysis was performed to study the stress and strain changes during the 2-2 coal and 2-1 coal mining process. During the mining of 2-2 coal, the large cycle weighting step distance of the working face is shorter than that of 2-1 coal, which indicates that the mining of the 2-2 coal working face is affected by the pressure relief of 2-1 coal. Furthermore, the mining of 2-1 coal has weakened the overburden structure, reducing the limit span of the suspended roof in the key thick sandstone stratum. The large period weighting strength of the working face during the mining of the 2-2 coal seam is lower than that of the 2-1 coal seam, which indicates that 2-2 coal is located in the lower part of the goaf

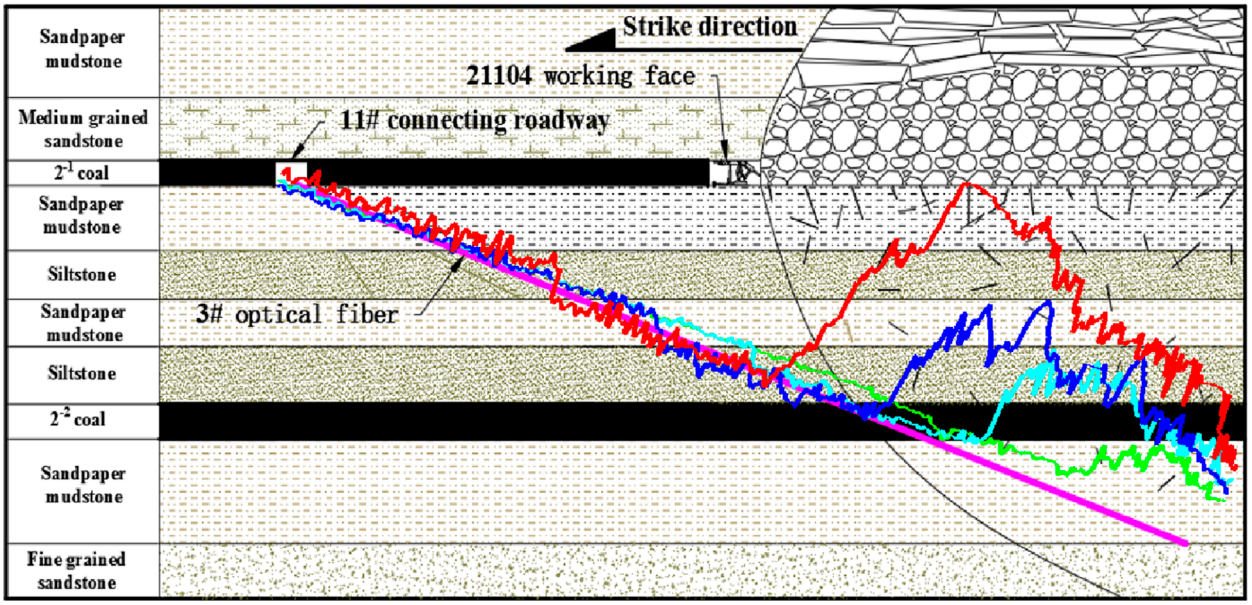

FIGURE 10
Schematic diagram of changes in the lower coal and rock mass during the mining process of the upper protective layer monitored by distributed fiber-optic sensing technology.

TABLE 3 Comparison of pressure relief parameters during upper stress-concentration stratum mining.

Classification	Numerical calculation	Engineering measurement
Stress-relieving angle of the protected coal seam along the direction of the strike/°	79.1–80.2	63.6
Stress-relieving angle of the protected coal seam in the dip direction/°	59.5–70.3	58.7
Proportion of the pressure relief of the protected coal seam along the direction of the strike/%	55.4	63.4–84.7
Proportion of the pressure relief of the protected coal seam in the dip direction/%	35.2–46.1	43.5–63.4
Stress-relieving hysteresis distance of the protected coal seam/m	10.0	14.3
Maximum depth of stress relief/m	32.8	28.4
Maximum depth of stress relief and distance from the work zone/m	35.5	38.5–40.5

during mining, making it easier for the goaf to be quickly filled. The breaking rotation space of the key thick sandstone stratum is reduced, and the breaking distance is shortened, so the energy released during the weighting of the working face is weakened. The results show that during the mining process of the protected layer, the degree of deformation caused by the collapse of the overlying rock is reduced, and the distance of the overlying rock roof and key thick sandstone layers from the hanging roof is reduced. The cyclic compression step distance and strength of the working face are also reduced, indicating that is the energy released by the rock layer fracture is reduced. Due to the uneven collapse of gangue in the goaf after the mining of the upper protective layer, the fully collapsed compacted area and the partially collapsed compacted area are alternately distributed, resulting in inconsistent strain recovery in the goaf and uneven distribution of underlying coal and rock unloading pressure. The unloading zone, stress recovery zone, and pressure-boosting zone are alternately distributed in the goaf. The research results provide a certain theoretical and scientific basis and technical guidance for the scientific and rational development and layout of close-range coal seam groups in mines, which has

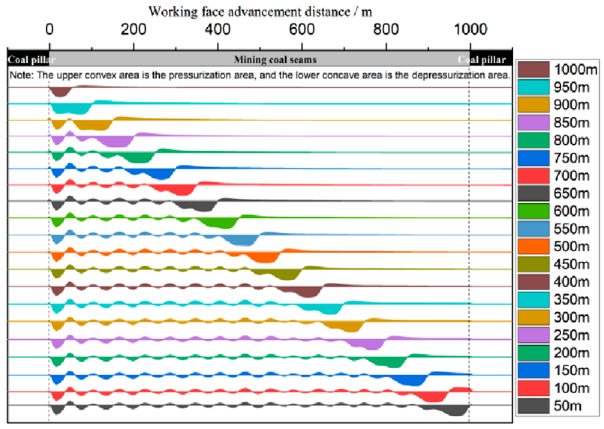

FIGURE 11
Schematic diagram of the dynamic evolution law of the vertical stress distribution in the direction of the protected layer 2-2 coal during the mining process of the upper protective layer.

important practical significance for the prevention and control of rockburst disasters in protective layer mining.

Fiber-optic sensing technology has enabled real-time monitoring of the pressure relief patterns and range of the underlying coal and rock mass during the mining process of the protective layer. The fiber-optic monitoring data reflect the dynamic process of stress increase, compression deformation, stress reduction, expansion deformation, and stress recovery, as well as tensile deformation reduction in the underlying coal rock mass during the mining process of the protective layer. Based on the fluctuation amplitude of the fiber-optic strain increment to characterize the pressure relief effect, the pressure relief process is divided into three stages, namely, the pressure relief start stage, the pressure relief active stage, and the pressure relief decay stage. This study aims to provide technical support for implementing pressure relief and anti-collision strategies in the mining of protective layers and explore the reliability of using fiber-optic sensing technology to monitor the pressure relief effect in protective layer mining. These findings are significant for the promotion and application of fiber optic sensing technology in the field of mining engineering.

According to the abovementioned research, when implementing protective layer mining to prevent and control rockburst disasters, the following issues should be emphasized:

(1) Selection and development layout of protective layer: When mining coal seams with the risk of rockburst, the protective layer should be first mined to prevent rockburst, and coal seams with no or weak rockburst risk should be selected as the protective layer as much as possible, with priority given to the upper protective layer. When dividing mining areas, it is necessary to ensure a reasonable mining sequence and minimize the formation of stress concentration areas such as coal pillars. The mining of the protective layer should be ahead of the mining of the protected layer to ensure that the protected layer is in a depressurized state.
(2) Mining technology and process optimization: When mining the protective layer, the longwall mining method should be used as much as possible, and the full collapse method should be used to manage the roof of the goaf. During the mining process of the protective layer, coal pillar-free mining technology should be adopted as much as possible to avoid leaving coal pillars in the goaf and reduce stress concentration.

9 Conclusion

(1) The stress changes in the underlying rock–coal strata during the mining of the upper stress-concentration stratum can be divided into four phases, namely, *in situ* stress, stress concentration, stress release, and stress recovery. At the same time, the strata undergo dynamic processes such as "pressure boosting, unloading development, unloading recovery, and unloading stability."
(2) After mining of the upper protective layer, the distribution of the gangue collapse in the goaf is divided into fully collapsed and compacted areas and partially collapsed areas. The stress in the goaf alternates between the stable unloading area, the recovery unloading area, and the pressure-increasing area. The stress distribution curve of the protected layer changes from a "U"-shape to a "W"-shape and then to a "WWW"-shape.
(3) The initial pressure relief peak step distance for the upper protective layer mining is 80 m, the periodic pressure relief peak step distance is 60 m, the initial pressure relief recovery step distance is 140 m, and the periodic pressure relief recovery step distance is 70 m. The pressure relief ratio in the goaf direction is 55.5%, and the pressure relief ratio in the dip range is 35.3%–46.2%.
(4) The numerical simulation calculation results of the stress-relieving parameters for the upper stress-concentration stratum mining are basically consistent with the engineering measurement results. This indicates that using the 2-1 coal seam as a stress-concentration stratum for mining in the Hulusu mine can have a pressure relief effect on the 2-2 coal seam. Thus, the stress-relieving effect of the stress-concentration stratum opening has significant time and space effects.

Data availability statement

The original contributions presented in the study are included in the article/Supplementary Material; further inquiries can be directed to the corresponding author.

Author contributions

WL: conceptualization, formal analysis, writing–original draft, and writing–review and editing. JC: project administration and writing–review and editing. CZ: data curation, formal analysis, and writing–review and editing. JZ: data curation, formal analysis, and writing–review and editing. SW: writing–review and editing. GL: writing–review and editing. JZ: methodology and writing–review and editing. RY: methodology and writing–review and editing.

Funding

The author(s) declare that financial support was received for the research, authorship, and/or publication of this article. This work is supported by the National Natural Science Foundation of China (No. 52264007), the Longyuan Youth Innovation and Entrepreneurship Talent (Team) Project, the Youth Doctoral Support Project for Universities in Gansu Province (2025QB-093), and Enterprise Research Projects (No. HXZK2344).

Conflict of interest

The authors declare that the research was conducted in the absence of any commercial or financial relationships that could be construed as a potential conflict of interest.

Generative AI statement

The author(s) declare that no Generative AI was used in the creation of this manuscript.

Publisher's note

References

Banerjee, B. D. (1987). A new approach to the determination of methane content of coal seams. *Geotechnical Geol. Eng.* 5 (4), 369–376. doi:10.1007/bf01552751

Blair, S. C., and Cook, N. G. W. (1998). Analysis of compressive fracture in rock using statistical techniques: Part II. Effect of microscale heterogeneity on macroscopic deformation. *Int. J. Rock Mech. Min. Sci.* 35 (7), 849–861. doi:10.1016/s0148-9062(98)00009-6

Cao, Z., He, X., Wang, E., and Kong, B. (2018). Protection scope and gas extraction of the low-protective layer in a thin coal seam: lessons from the DaHe coalfield, China. *Geosciences J.* 22 (3), 487–499. doi:10.1007/s12303-017-0061-1

Chen, S., Shi, B., Mu, C., and Lu, Z. (2013). Study on seam permeability - increased effects and pressure - relaxed range during protective seam mining. *Coal Sci. Technol.* 41 (04), 45–49.

Chen, X., Sheng, G., and Gao, Z. (2024). Study on the influence of coal pillar left by long-distance mining of protected layer on the mining of protected layer. *Saf. Coal Mines* 55 (3), 46–52.

Cundall, P. A. (1976). Explicit finite-difference methods in geomechanics. *Numer. Methods Geomechanics* 1, 132–150.

Dai, G., Guo, L., and Zhang, S. (2013). Numerical simulation of haizi mine upper protective layer mining's protection scope. *China Saf. Sci. J.* 23 (07), 13–18.

Fang, F., Shu, C., and Wang, H. (2020). Physical simulation of upper protective coal layer mining with different coal seam inclinations. *Energy Sci. & Eng.* 8 (9), 3103–3116. doi:10.1002/ese3.740

Gong, P., Hu, Y., Zhao, Y., and Yang, D. (2005). Three dimensional simulation study on law of deformation and breakage of coal floor on mining above aquifer. *Chin. J. Rock Mech. Eng.* 24 (12), 4396–4402.

Guan, J., Sun, K., and Zhu, Y. (2002). Study of rockburst prevention and its numerical simulation in slant coalbed. *J. Liaoning Tech. Univ. Sci.*, 411–413.

Guan, Y., Li, H., and Fan, Z. (2008). Similar material simulation of the failure law of coal seam floor. *Saf. Coal Mines* 2, 67–69.

Jiang, F., Liu, Y., Liu, J., Zhang, M., Du, J., Sun, W., et al. (2019). Pressure-releasing mechanism of local protective layer in coal seam with rock burst. *Chin. J. Geotechnical Eng.* 41 (02), 368–375.

Jiang, Y., and Zhao, Y. (2015). State of the art:investigation on mechanism, forecast and control of coal bumps in China. *Chin. J. Rock Mech. Eng.* 34 (11), 2188–2204.

Kang, H., Gao Fuqiang, Xu Gang, Ren Huaiwei, (2023). Mechanical behaviors of coal measures and ground control technologies for China's deep coal mines - a review. *J. Rock Mech. Geotechnical Eng.* 15 (1), 37–65. doi:10.1016/j.jrmge.2022.11.004

Lan, H., Chen, D., and Mao, D. (2016). Current status of deep mining and disaster prevention in China. *Coal Sci. Technol.* 44 (01), 39–46.

Lei, W., Chai, J., Ding, G., Zhang, Y., Yao, R., and Wang, L. (2024). Industrial experimental study on fiber optic sensing of pressure relief effect in coal and rock mining with upper urotective layer. *Min. Res. Dev.* 44 (4), 130–137.

Lei, W., Chai, J., Zhang, Y., Ding, G., Yao, R., Chen, Y., et al. (2022). Study on pressure relief effect of upper protective coal seam mining based on distributed optical fiber sensing monitoring. *Opt. Fiber Technol.* 68, 102830–102915. doi:10.1016/j.yofte.2022.102830

Li, J., Tian, Y., Yan, X., Xie, K., Wang, Y., Xu, W., et al. (2020). Approach and potential of replacing oil and natural gas with coal in China. *Front. Energy* 14 (2), 419–431. doi:10.1007/s11708-020-0802-0

Li, P., Chen, Y., Wang, L., and Ren, W. (2012). Similar simulation experiment of the released range of upper protective seam mining. *Saf. Coal Mines* 43 (12), 32–36.

Li, X., Chen, S., Wang, S., Zhao, M., and Liu, H. (2021). Study on *in situ* stress distribution law of the deep mine: taking linyi mining area as an example. *Adv. Mater. Sci. Eng.* 2021, 1–11. doi:10.1155/2021/5594181

Li, X., Chen, S., and Zhang, X. (1997). Research on the application of protective layer mining to prevent and control rockburst. *J. Min. And Strata Control Eng.*, 18–20.

Lin, Q., Cao, P., Wen, G., Meng, J., Cao, R., and Zhao, Z. (2021). Crack coalescence in rock-like specimens with two dissimilar layers and pre-existing double parallel joints under uniaxial compression. *Int. J. Rock Mech. Min. Sci.* 139, 104621–104714. doi:10.1016/j.ijrmms.2021.104621

Liu, H., Hao, C., Wang, Z., Li, C., Guo, L., Liang, J., et al. (2022). Study on stability of underlying room and pillar old goaf in close coal seam and mining of the upper coal seam. *Front. Earth Sci.* 10, 1–14. doi:10.3389/feart.2022.1071250

Liu, J., Zhang, X., and Zhang, X. (2023). Study on spatial and temporal evolution law of surrounding rock stress in mining of upper and lower protective layers of coal seams group and its application. *J. Saf. Sci. Technol.* 19 (6), 66–73.

Lv, H., Cheng, Z., Xie, F., Pan, J., and Liu, F. (2024). Study on hydraulic fracturing prevention and control of rock burst in roof of deep extra-thick coal seam roadway group. *Sci. Rep.* 14 (1), 29537. doi:10.1038/s41598-024-77363-0

Mu, H., Zhang, Y., Gao, M., Zhu, Q., Li, J., Cao, J., et al. (2024). Research on the attenuation characteristics of seismic energy in multicoal seam mining and the warning method of rock burst. *Energy Sci. & Eng.* 12 (11), 4932–4949. doi:10.1002/ese3.1904

Pang, L., Xu, X., Si, L., Zhang, H., and Li, Z. (2016). Analysis of prevention mechanism of upper protective seam mining on rock rockburst induced by thick conglomerate. *Rock Soil Mech.* 37 (S2), 120–128.

Shen, R., Wang, E., Liu, Z., and Li, Z. (2011). Rockburst prevention mechanism and technique of close-distance lower protective seam mining. *J. China Coal Soc.* 36 (S1), 63–67.

Shen, W., Dou, L., He, H., and Zhu, G. (2017). Rock burst assessment in multi-seam mining: a case study. *Arabian J. Geoences* 10 (8), 196–211. doi:10.1007/s12517-017-2979-z

Shi, Z., Ye, D., Qin, B., Hao, J., Sun, W., and Fang, S. (2022). Mining height effect and application of upper protected layer mining pressure relief. *Sustainability* 14 (16), 10119–10218. doi:10.3390/su141610119

Sitao, Z., Decheng, G., Fuxing, J., Wang, C., Li, D., Shang, X., et al. (2021). Rock burst mechanism under coupling action of working face square and regional Tectonic stress. *Shock Vib.* 2021, 21–11. doi:10.1155/2021/5538179

Sun, R., Jiang, Z., Li, X., Yao, H., and Sun, Q. (2013). Study on the failure depth of thick seam floor in deep mining. *J. China Coal Soc.* 38 (1), 67–72.

Tian, K., Tang, X., Liu, Z., and Zheng, J. (2014). Analysis on protection effect of upper protective seam mining and fractured zone. *Coal Eng.* 46 (04), 71–73.

Tu, M., Huang, N., and Liu, B. (2007). Research on pressure - relief effect of overlying coal rock body using far distance lower protective seam Exploitation method. *J. Min. & Saf. Eng.*, 418–421.

Wang, H., Xu, L., Yu, H., and Zhang, J. (2024). Research on prediction of high energy microseismic events in rock burst mines based on BP neural network. *Sci. Rep.* 14 (1), 29934. doi:10.1038/s41598-024-81614-5

Xiao, Z., Liu, J., Gu, S., Liu, M., Zhao, F., Wang, Y., et al. (2019). A control method of rock burst for dynamic roadway floor in deep mining mine. *Shock Vib.* 2019, 1–16. doi:10.1155/2019/7938491

Xie, H., Gao, M., Zhang, R., Peng, G., Wang, W., and Li, A. (2019). Study on the mechanical properties and mechanical Response of coal mining at 1000m or deeper. *Rock Mech. Rock Eng.* 52 (05), 1475–1490. doi:10.1007/s00603-018-1509-y

Xiong, Z., Tao, G., and Yuan, G. (2014). Pressure relief boundary of protected seam mining with subhorizontal long-distance. *J. Xi'an Univ. Sci. Technol.* 34 (02), 147–151.

Xu, G., Wang, L., Jin, H., and Wang, Q. (2019). Study on movement deformation laws and protection effect of lower ultra-thick coal seam affected by upper protective layer mining. *J. Saf. Sci. Technol.* 15 (06), 36–41.

Xu, L., Lu, K., Pan, Y., and Qin, Z. (2019). Study on rock burst characteristics of coal mine roadway in China. *Energy Sources Part A Recovery Util. Environ. Eff.* 44, 3016–3035. doi:10.1080/15567036.2019.1655114

Xuanhong, D., Junhua, X., Lan, Y., Wulin, L., Hengfei, M., Chen-Rui, C., et al. (2024). Coal damage and energy characteristics during shallow mining to deep mining. *Energy* 291, 1–13.

Yang, T. (2024). Recognition and prediction of precursory feature signals of coal mine rock burst based on random forest and MK trend test. *Front. Comput. Intelligent Syst.* 8 (3), 1–5. doi:10.54097/5xwgxa77

Yu, Y., Geng, D., Tong, L., Zhao, X., Diao, X., and Huang, L. (2018). Time fractal behavior of microseismic events for different intensities of immediate rock bursts. *Int. J. Geomechanics* 18 (7), 1–11. doi:10.1061/(asce)gm.1943-5622.0001221

Yuan, H., Ji, S., Li, H., Zhu, C., Zou, Y., Ni, B., et al. (2024). Classification forecasting research of rock burst intensity based on the BO-XGBoost-Cloud model. *Earth Sci. Inf.* 18 (1), 95. doi:10.1007/s12145-024-01596-w

Yuan, Z. G., Shao, Y. H., and Zhu, Z. H. (2019). Similar material simulation study on protection effect of steeply inclined upper protective layer mining with varying interlayer distances. *Adv. Civ. Eng.* 2019, 1–14. doi:10.1155/2019/9849635

Zhang, H., Fu, X., Huo, B., Lu, Y., and Zhou, K. (2017). On preparing the materials as close as possible in the experimental ratio and mechanical properties with those gained from mining. *J. Saf. Environ.* 17 (06), 2134–2139.

Zhu, Y., Zhang, Y., and Pan, Y. (2003). Feasible research on prevention of rock-burst in dip-slopping coal seam. *J. Liaoning Tech. Univ. Sci.*, 332–333.

Zhu, Z., Wu, Y., and Han, J. (2021). A prediction method of coal burst based on analytic hierarchy process and fuzzy comprehensive evaluation. *Front. Earth Sci.* 9, 1–12. doi:10.3389/feart.2021.834958